Available online at www.sciencedirect.com

SCIENCE DIRECT®

ELSEVIER

Palaeogeography, Palaeoclimatology, Palaeoecology 226 (2005) 72–92

PALAEO

www.elsevier.com/locate/palaeo

Climate shift at 4400 years BP: Evidence from high-resolution diatom stratigraphy, Effingham Inlet, British Columbia, Canada

Alice S. Chang*, R. Timothy Patterson

Department of Earth Sciences, Carleton University, 1125 Colonel By Drive, Ottawa, Ontario, Canada K1S 5B6

Received 5 January 2005; received in revised form 3 May 2005; accepted 10 May 2005

Abstract

Diatom paleoecology and climatic interpretations were assessed from a 15-cm long laminated sediment slab extracted from an anoxic fjord in southwest British Columbia. The slab spans at least 62 years of deposition, determined from counting varves, and is dated at approximately 4400 years BP. The slab shows a sedimentation pattern where thick diatom-rich varves at the bottom become thinner and more silty toward the top. Thin section analysis reveals that the thicker varves contain a distinct succession of diatoms, representing seasonal deposition throughout each year. Annual-scale subsampling shows that the abundance of coastal marine diatoms, namely a weakly silicified form of *Skeletonema costatum*, decreased over the 62-year period, while benthic and brackish water diatoms, such as *Planothidium delicatulum* and *Achnanthes minutissima*, increased with the concomitant increase in silt. The increase in such benthic species and silt, along with the presence of ~1 cm thick nonlaminated intervals, is interpreted to represent deposition during progressively increasing precipitation over time. These sedimentation patterns and changes in diatom assemblages may signify a change in the relative intensities of the Aleutian Low (AL) and North Pacific High (NPH) atmospheric pressure systems. Thicker diatomaceous varves at the bottom of the slab reflect a stronger NPH system with associated coastal upwelling and enhanced diatom production. The thinner silty varves at the top of the slab suggest that the AL system was prevalent, resulting in greater amounts of precipitation and reduced upwelling. The findings of this study show that significant natural environmental change can occur within a twenty-year time frame, and can provide a basis for the study of modern change in the ocean–atmosphere system over the northeast Pacific Ocean.

Keywords: Diatoms; Laminated sediments; Paleoecology; Stratigraphy; Climate change; Oceanography; Holocene; Northeast Pacific

1. Introduction

Assessing modern climate and environmental change is of utmost importance as society becomes increasingly aware of the sensitive balance in natural systems. In the 21st century, understanding the

* Corresponding author. Current address: School of Earth and Ocean Sciences, University of Victoria, PO Box 3055 Stn CSC, Victoria, British Columbia, Canada V8W 3P6. Tel.: +1 250 472 5345; fax: +1 250 721 6200.

E-mail address: asm_chang@yahoo.com (A.S. Chang).

0031-0182/$ - see front matter © 2005 Elsevier B.V. All rights reserved.
doi:10.1016/j.palaeo.2005.05.004

causal factors involved in rapid (decadal to bidecadal) change can be challenging because anthropogenic and natural signals need to be differentiated. Although instrumental records exist for the last ~150 years and can be compared to contemporary sediments to determine the relationship between climate, primary production and depositional patterns, these modern sediment records can be tainted from the effects of industrialization. Hence, older sediments from the pre-industrial era must be used to provide a natural baseline.

Large-scale ocean–atmosphere oscillations such as the El Niño-Southern Oscillation, the Pacific Decadal Oscillation (Mantua et al., 1997) and the 50–70 year oscillation (Minobe, 1999) can have a profound influence on climate over the northeast Pacific Ocean and biological production off the coast of British Columbia. For 20th century records, primary production and fish migratory patterns were observed to oscillate between warm and cool climate phases in the northern Pacific (Mantua et al., 1997; Chavez et al., 2003). These shifts in production have a major impact on coastal communities that rely on the commercial harvesting of economic fish species. It is therefore important to understand the causes and timing of these productivity cycles. One way to investigate this issue is to determine whether such changes have occurred previously, or are recurring phenomena, by looking into the sediment record. Recent studies of finely laminated sediments in the fjords of Vancouver Island, British Columbia, have utilized high-resolution imaging and/or statistical techniques in order to resolve late Holocene depositional and climate patterns (e.g., Dean et al., 2001; Chang et al., 2003; Dean and Kemp, 2004; Patterson et al., 2004a). These studies reveal that there are a multitude of climate cycles that have left an imprint within the sediments for at least the last 4500 years.

In this paper, we examine a high-resolution laminated sediment record and primary production proxy from Effingham Inlet, southwest Vancouver Island, by determining diatom abundance and assemblages and measuring changes in lamina thickness. Thin sections and successive annual samples were extracted from a 15-cm long sediment slab that encompasses at least 62 years of deposition and was dated at approximately 4400 years BP (Chang et al., 2003). The objectives of this study are to (1) describe the seasonal components of the sediments from thin section analysis, (2) present quantitative results from the enumeration of diatoms, and (3) interpret past climatic and oceanographic trends derived from the sedimentation patterns and diatom assemblages. The results of this study should be able to provide a foundation for comparison to modern sediments from similar depositional environments.

2. Regional climate and oceanography today

The modern coastal climate of southwest Vancouver Island is cool-temperate and precipitation can reach up to 250 cm annually (Ryder, 1989). Winters are relatively cool and rainy, and the coastal region is affected by a succession of frontal systems associated with cyclonic storms. Coastal air temperatures are mild, ranging from 1 to 5 °C. Summers are relatively warmer and drier, and the coastal region is influenced by large anticyclonic systems. Air temperatures can reach up to 20 °C.

The dominant surface currents seaward of the continental slope of North America are the northward-flowing Alaska Current and the southward-flowing California Current (Thomson, 1981). Over the continental slope and outer shelf of Vancouver Island, the surface currents are seasonally variable in response to the prevailing winds (Fig. 1A). In the winter, the Northeast Pacific Coastal Current flows northwestward in response to winds associated with the counterclockwise circulation of the Aleutian Low (AL) atmospheric pressure system (Thomson, 1981; Thomson and Gower, 1998). In the summer, the current flows southeastward as the "shelf-break current" in response to winds associated with the clockwise circulation of the North Pacific High (NPH) pressure system (Thomson and Gower, 1998). Flow over the inner shelf is dominated by the buoyancy-driven Vancouver Island Coast Current (Thomson et al., 1989). This current is driven primarily by brackish water outflow from Juan de Fuca Strait and flows to the northwest throughout the year (Fig. 1B).

Wind-induced annual upwelling along the west coast of Vancouver Island is most prevalent from May through August. The upwelling extends seaward of the 200-m shelf break, with subsequent transport of deeper (>150 m) oxygenated and nutrient-rich slope waters onto the outer shelf (Thomson et al., 1989).

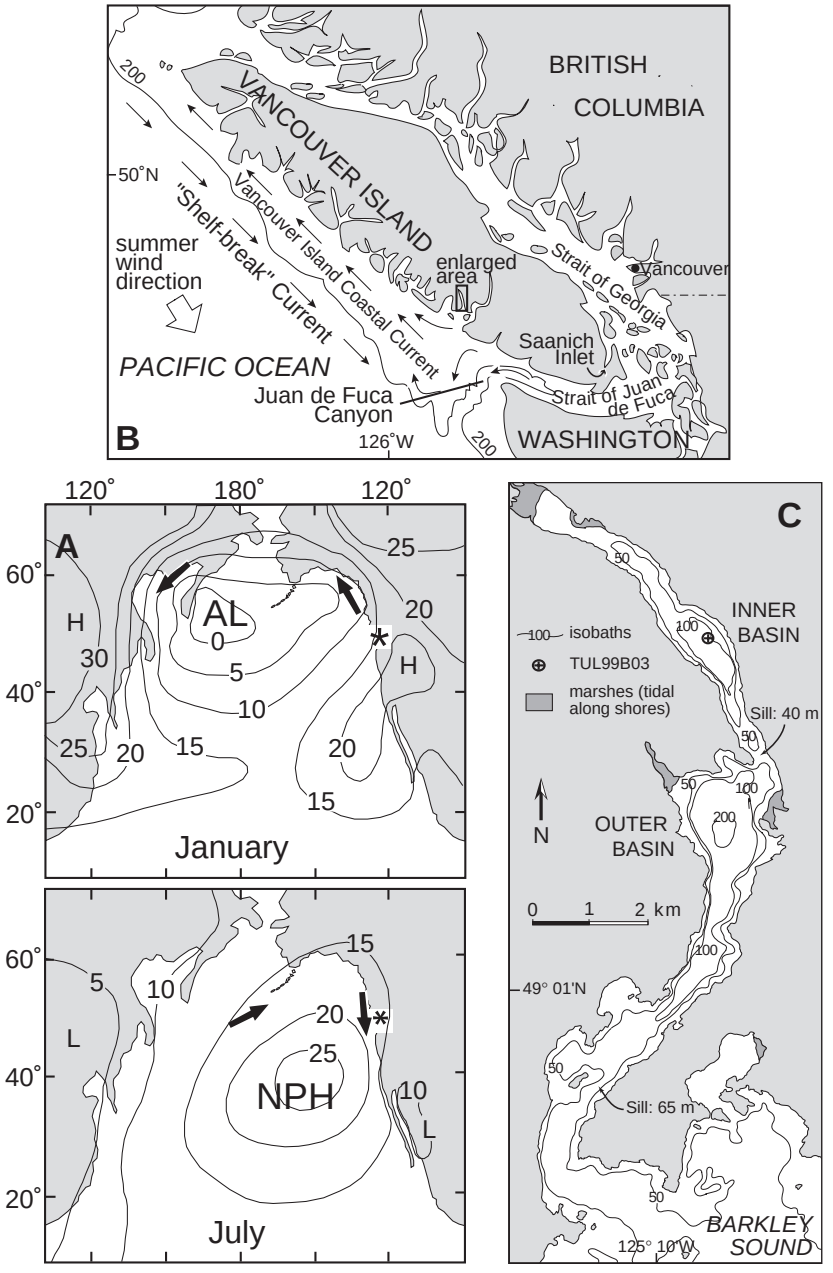

Fig. 1. (A) The Aleutian Low (AL) and North Pacific High (NPH) atmospheric gyres and prevailing wind directions (arrows) during winter (January) and summer (July). Asterisks mark location of study area. Values + 10,000 divided by 10 gives pressure in millibars. After Favorite et al. (1976). (B) Regional map showing summer surface currents, wind direction, other oceanographic features, and location of Effingham Inlet (box). (C) Detail of Effingham Inlet and location of core TUL99B03 from the inner basin. Isobaths in (B) and (C) in meters.

The upwelled waters then move directly shoreward over the shelf (or indirectly shoreward following northward transport within deep troughs extending northward from Juan de Fuca Canyon) where they can lead to a marked increase in phytoplankton production in the adjoining coastal inlets. The seasonal

upwelling is initiated in response to a seaward, wind-forced Ekman transport in the surface layer and coincides with the southeastward-flowing shelf-break current (Fig. 1B). This spring/summer flow structure is, in turn, driven by clockwise circulating winds associated with the NPH pressure system (Thomson and Gower, 1998).

3. Effingham Inlet

Effingham Inlet opens to the Pacific Ocean via Barkley Sound (Fig. 1C). The shoreline is mostly steep and rocky except for low-lying marshy areas. The fjord measures 17 km in length, has an average width of 1 km, and contains two bedrock sills and two basins. Like most fjords on Vancouver Island, Effingham Inlet is classified as a low-runoff fjord (Pickard, 1963). Peak discharge in Effingham Inlet occurs during the winter months when precipitation is at a maximum. A combination of small spring snowmelt and low discharge produces weaker estuarine circulation during the summer months than in the winter months. However, salinity and oxygen data indicate that Effingham Inlet experiences well-developed estuarine-type stratification throughout the year, with a year-round layer of fresh water at the surface (Patterson et al., 2000). This suggests that there must be sufficient precipitation during the summer to maintain a high enough flow so that estuarine circulation does not break down. The restricted nature of the fjord, estuarine stratification, and high primary production lead to anoxia of the bottom waters within the inner basin, and dysoxia of the bottom waters in the outer basin. The low oxygen content of the bottom waters excludes bioturbating macrobenthos and allows for the preservation of finely laminated sediments consisting mainly of clay and silt size components. A brown-colored detritus-rich lamina, deposited during the autumn and winter, and an olive-colored diatom-rich lamina, deposited during the spring and summer, comprise an annual varve. A lack of physical and biological reworking of these sediments permits the preservation of a high-resolution environmental archive.

Because the bottom water salinity of the outer basin is higher than that at the outer sill, it may be inferred that seawater of higher salinity and density occasionally breaches the sill and spills into the basins. Such seawater incursions presumably occur during the winter, under the influence of strong northerly winds at the time of Arctic outbreak conditions (Patterson et al., 2000), or early in the annual spring upwelling season during a rare combination of weak tidal currents in the fjord, significant rainfall, and strong (>10 m s^{-1}) northeasterly winds (Thomson, 1981). The inflowing seawater has the effect of periodically oxygenating the bottom waters of both basins. Such an "oxygenation event" was witnessed in January and July 1999, with normal anoxia returning within a few months of each event.

4. Methods and materials

Piston core TUL99B03 (49° 04.275′ N, 125° 09.359′ W; 11.4 m long, 10 cm diameter; 120 m water depth) was recovered from the inner basin of Effingham Inlet in 1999 (Fig. 1C). The majority of the core contains visibly distinct sedimentary laminae, with thin (<10 cm) nonlaminated intervals intercalated throughout the core. The core was AMS radiocarbon dated with two shell dates and four wood dates (Dallimore, 2001). The dates were calibrated using the program C14CAL98 (Stuiver and Reimer, 1993; Stuiver et al., 1998a,b) along with the dendrochronologically derived INTCAL98 dataset for terrestrial material and the MARINE98 dataset for marine material (Stuiver et al., 1998a,b). A locally determined marine reservoir correction of -125 ± 45 yr (Dallimore, 2001) was used, and the core was determined to span in age from ~500–5500 years BP (Chang et al., 2003; Patterson et al., 2004b).

A 15-cm long slab (called Slab 8) from core depth 870–885 cm was extracted for high-resolution stratigraphic analysis because its distinct laminae and varves which show a thinning upward sequence. The slab has been previously X-rayed to reveal its internal structures and bulk density variations (Chang et al., 2003). No exact radiocarbon age was determined for this slab, so by assuming a constant sedimentation rate and using linear interpolation, this slab was dated at approximately 4400 years BP (Chang et al., 2003). The sediments immediately above and below this slab are laminated.

A 5-mm wide sediment strip was sliced perpendicular to laminae along the edge of Slab 8 and embedded with Spurr low-viscosity epoxy resin for the production of a continuous set of thin sections. The embedding technique is similar to the procedure of Lamoureux (1994). During the embedding process, the top 1.3 cm of the sediment strip was damaged and discarded. The successfully embedded sediments were cured, sectioned diagonally into approximately 3-cm long pieces with a bandsaw, and polished into thin section slides. Five slides were produced and photographed at a magnification of 12× using an Olympus SZH-10 stereo microscope and a digital microscope camera. Lamina thickness measurements and varve boundaries were determined from the photographs.

Sediment texture and composition were described by examining the thin sections at 400× on a petrographic microscope in plane polarized light. The abundance of microfossils and other particles were semi-quantitatively assessed by visually estimating the percentage proportion of the microfossil or particle per field of view per lamina. The percentage estimates and compositions were then used to classify laminae as either terrigenous or diatomaceous, where the latter can be further divided into near-monospecific, mixed-species or silty diatomaceous laminae. Terrigenous laminae contain mainly silt and organic detritus, with a minor component of robust diatoms, silicoflagellates and diatom fragments. Near-monospecific laminae consist mainly of a near-monospecific diatom assemblage; silt and organic detritus are absent. Mixed species laminae contain a diverse diatom assemblage and a minor component of silt and organic debris. Silty diatomaceous laminae also contain a diverse diatom assemblage, but the silt and organic debris content is greater than in mixed-species laminae. Dinoflagellate cysts and silicoflagellate tests have been observed in increased abundance in silty diatomaceous laminae (Chang et al., 2003).

A scalpel was used to sample individual varves from the remainder of the slab for annually time-averaged estimates of diatom abundance and composition. Thin (~1 cm) nonlaminated intervals and indistinct varves were also sampled, giving a total of 67 subsamples. The samples were freeze dried and processed by transferring ~40 mg of dry sediment into 20-mL glass scintillation vials. Sediments were treated with 10% hydrochloric acid and 30% hydrogen peroxide and heated on a hotplate until the organic matter was digested. A 4 g/L solution of sodium polyphosphate was added to each sample to disperse clay minerals. The supernatant from each vial was decanted each day for five days. After each decantation, the vials were filled with distilled water.

Diluted sediment slurry was plated using strewnmount techniques. Plating was done by extruding and evenly distributing 500 μL of diluted slurry onto a pre-cleaned 18 × 18 mm cover slip using a calibrated micropipet. After drying, the cover slips were mounted onto glass slides with toluene-diluted Naphrax™ mountant (refractive index = 1.74).

Identification and enumeration of diatoms were carried out at 1000× magnification with an Olympus BX-51 research microscope equipped with a differential interference contrast filter. Diatom taxa were identified to species level. Identification was based mainly on the floras of Cumming et al. (1995), Bérard-Therriault et al. (1999), Campeau et al. (1999), and Witkowski et al. (2000). *Chaetoceros* spp. resting spores (CRS) were grouped together as a genus because although some species were recognizable, a majority could not be identified.

Diatoms were counted as valves (one half of a frustule) as were CRS (one half of a spore). At least 500 diatom valves were counted per sample. CRS were enumerated until the diatoms were fully counted. The counting of CRS will provide minimum values since not all vegetative cells produce spores (cf. Hemphill-Haley and Fourtanier, 1995). At least 30 fields of view were counted for all of the slides, except for three (samples S8-18, 36, and 50) where diatoms were more abundant. Diatom counting pro-

Fig. 2. Subsampling horizons and absolute abundances. (A) Thin section intervals (see Appendix A). (B) Varve intervals and labels (see Appendix A). (C) Positive X-radiograph of slab. Dark layers are terrigenous laminae and light layers are diatomaceous laminae. Laminae at the top and bottom of the image are blurry due to increased obliquity of X-ray beam from the center of source. (D) Sampling intervals and labels for diatom analysis. (E) Absolute abundance of total diatoms (black bars) and *Chaetoceros* spp. resting spores (gray bars) in millions of valves per gram of dry sediment.

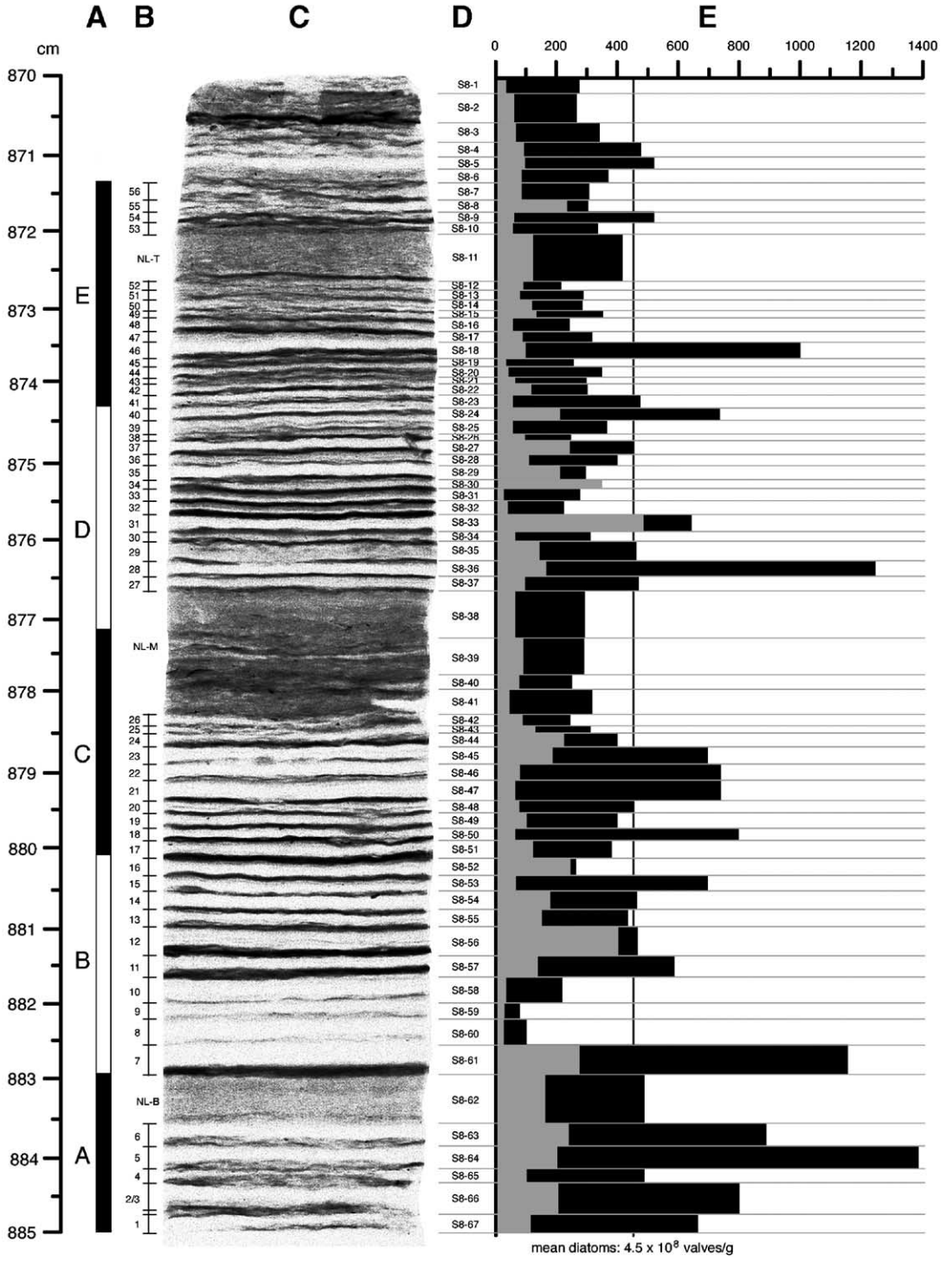
A
B
C
D
E
cm
870
871
872
873
874
875
876
877
878
879
880
881
882
883
884
885
E
D
C
B
A
NL-T
NL-M
NL-B
0
200
400
600
800
1000
1200
1400
S8-1
S8-2
S8-3
S8-4
S8-5
S8-6
S8-7
S8-8
S8-9
S8-10
S8-11
S8-12
S8-13
S8-14
S8-15
S8-16
S8-17
S8-18
S8-19
S8-20
S8-21
S8-22
S8-23
S8-24
S8-25
S8-26
S8-27
S8-28
S8-29
S8-30
S8-31
S8-32
S8-33
S8-34
S8-35
S8-36
S8-37
S8-38
S8-39
S8-40
S8-41
S8-42
S8-43
S8-44
S8-45
S8-46
S8-47
S8-48
S8-49
S8-50
S8-51
S8-52
S8-53
S8-54
S8-55
S8-56
S8-57
S8-58
S8-59
S8-60
S8-61
S8-62
S8-63
S8-64
S8-65
S8-66
S8-67
mean diatoms: 4.5 x 10^8 valves/g

cedures followed that of Laws (1983) and Schrader and Gersonde (1978).

The absolute abundance (concentration) of diatoms and CRS in each sample was calculated with the equation $C_a = Nadv_s/fAwv_p$, where C_a is the estimated absolute abundance of valves per gram of dry sediment, N is the total number of valves counted on the slide, a is the area of the cover slip, d is the dilution factor of the slurry plated to the cover slip, v_s is the initial volume (mL) of slurry used from the scintillation vial, f is the number of fields of view examined, A is the area of the field of view at 1000× magnification, w is the initial weight (g) of sediment used, and v_p is the volume (mL) of slurry plated onto the cover slip. The relative abundance (in percent) of individual diatom taxa was calculated by $C_r = (n_i/N)100$, where n_i is the number of valves for diatom taxon i counted in the sample, and N is the total number of valves counted in the sample.

5. Results

5.1. Sediment description

Slab 8 contains well-preserved varves showing a thinning upward trend (Fig. 2). At least 62 well-defined varves have been identified from visual inspection of the slab and from X-ray and thin section analyses. Varve thickness ranges from 0.75 to 3.53 mm, with a mean thickness of 1.82 mm ($n=56$) (Fig. 3). Varves 1–26 from the bottom of the slab average 2.22 mm in thickness (terrigenous=0.47 mm, diatomaceous=1.75 mm) whereas varves 27–56 from the top of the slab average 1.47 mm (terrigenous=0.37 mm, diatomaceous=1.10 mm). The thicker varves at the bottom of the slab contain thick diatom-rich laminae (thick bright layers in Fig. 2C). As the varves become thinner toward the top of the slab, diatomaceous laminae become thinner by an average of 37% and are more silty, and the thickness of the terrigenous laminae is reduced by an average of 21% (Fig. 3).

5.2. Diatom successions

The succession of diatom taxa was determined with thin section analysis. Although a yearly varve

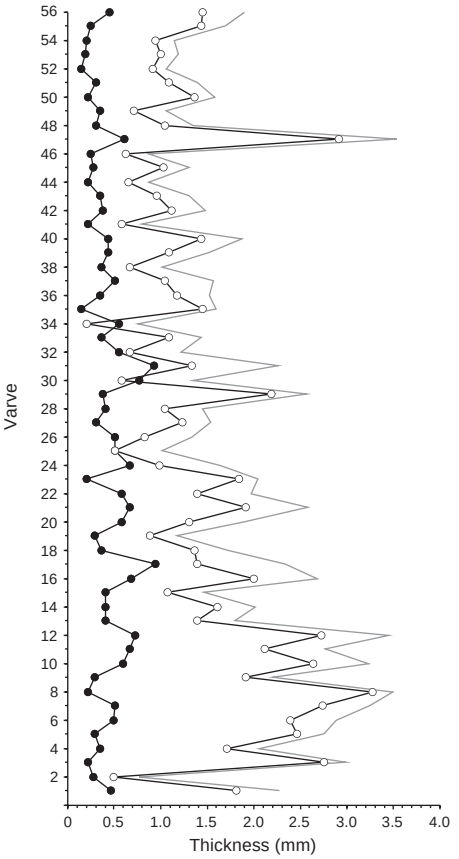

Fig. 3. Thickness of terrigenous laminae (closed circles), diatom-rich laminae (open circles), and combined total (gray line) determined from 56 varves from thin section measurements.

contains a terrigenous and a diatomaceous lamina, the diatomaceous lamina itself can be divided into component laminae based on taxonomic compositions (Chang et al., 2003). A general pattern of succession emerges: terrigenous laminae are typically overlain by discrete near-monospecific sublaminae containing *Thalassiosira* species, *Skeletonema costatum* or CRS, respectively. In some varves, these three taxa are mixed together into a single lamina. The sublaminae are then overlain by a mixed-species lamina, and finally by a silty diatomaceous lamina (Appendix A). Dinoflagellate cysts were found in the latter lamina type in varve 10 (Appendix A, Slide B). In some varves there is a near-monospecific lamina (containing *Asteromphalus* sp., CRS, *Odontella longicruris*, *S. costatum*, *Thalassionema nitzschioides*, or *Thalassiosira eccentrica*)

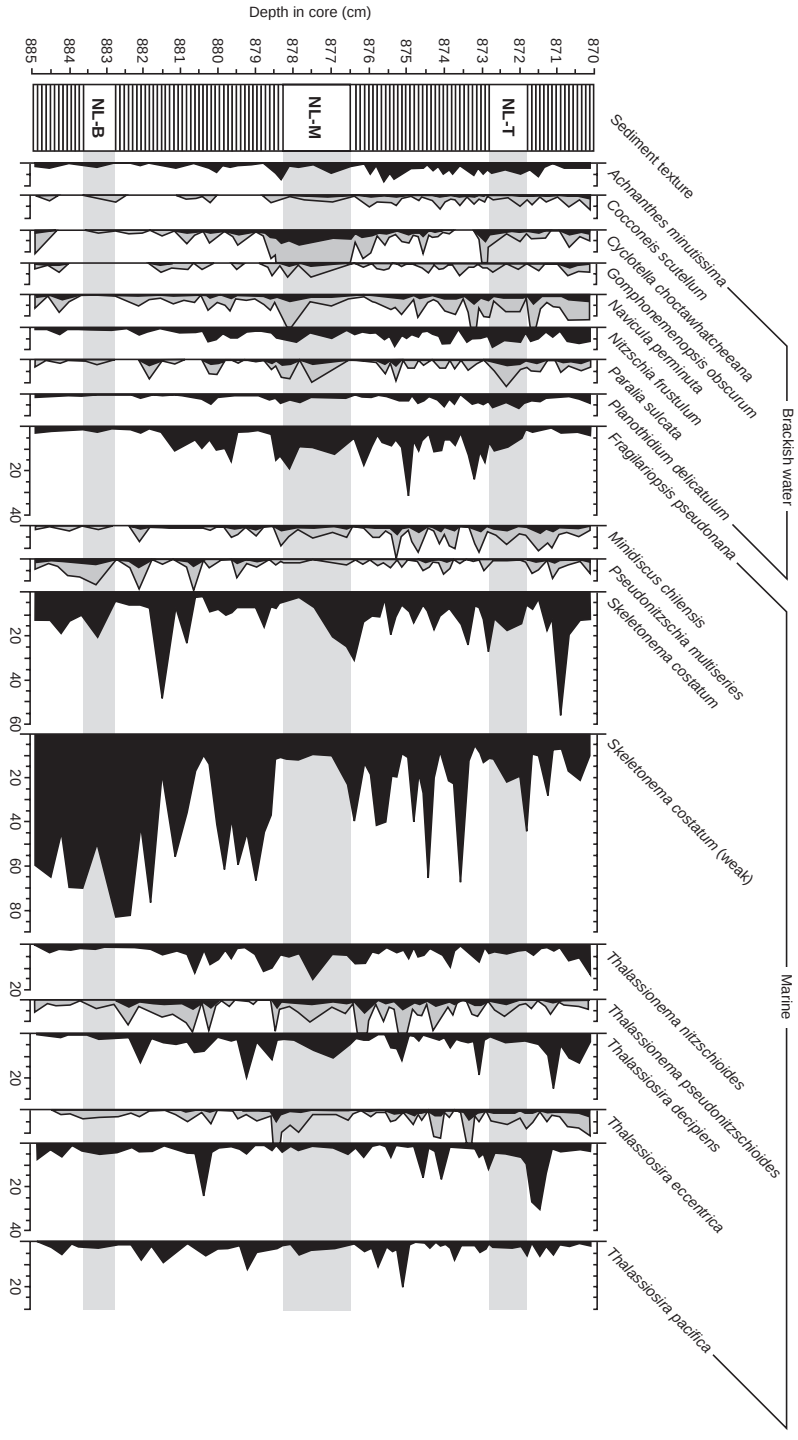

Fig. 4. Relative abundance (%) for selected major diatom taxa. Gray profiles represent percentages exaggerated by five times. Sediment texture: stripes = laminated. Nonlaminated intervals (NL) from the bottom (B), middle (M, including indistinct varves) and top (T) of the slab. Floral compositions of the nonlaminated intervals have been highlighted.

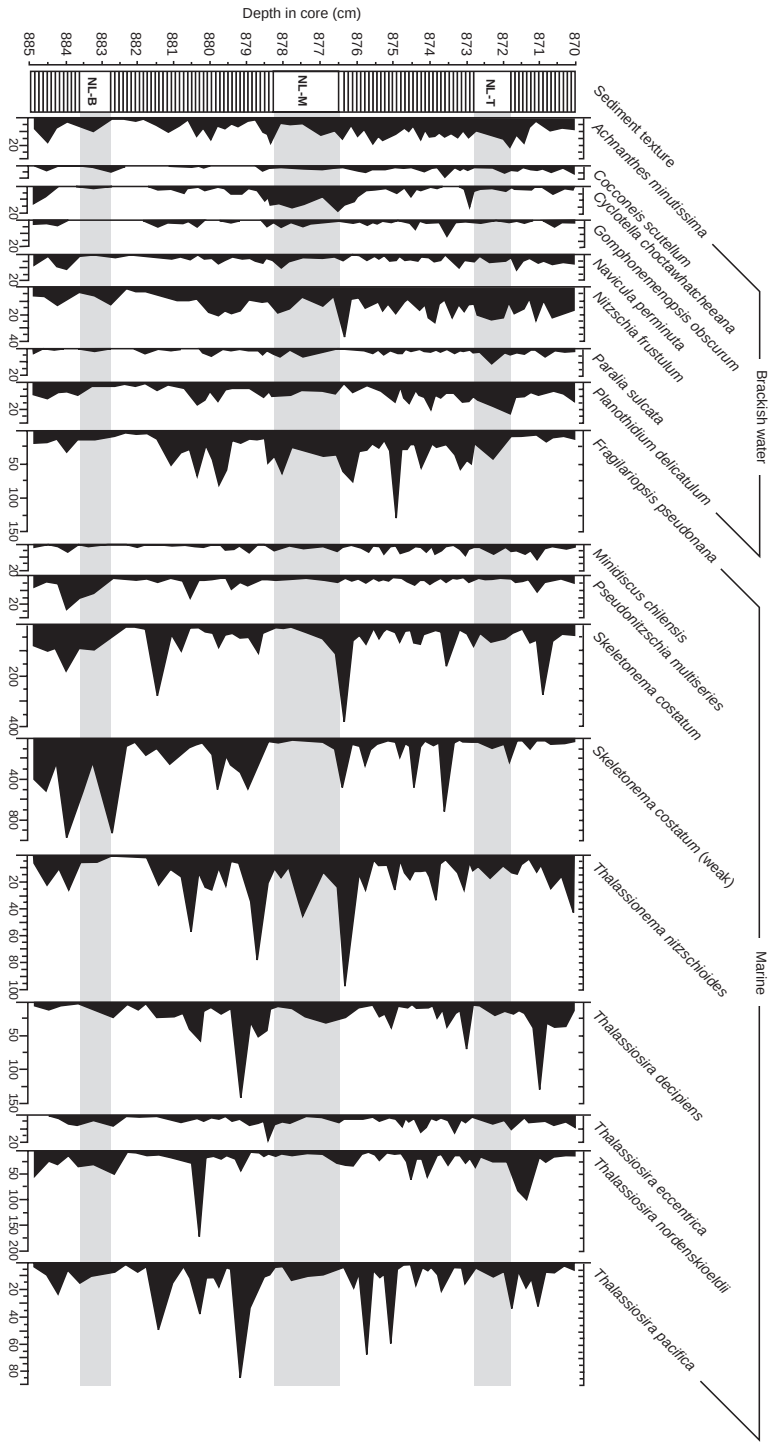

Fig. 5. Absolute abundance ($\times 10^6$ valves/g of dry sediment) for selected major diatom taxa. Sediment texture: stripes=laminated. Non-laminated intervals (NL) from the bottom (B), middle (M, including indistinct varves) and top (T) of the slab. Floral compositions of the nonlaminated intervals have been highlighted.

intercalated with the silty diatomaceous lamina (see Appendix A for varves 1, 6, 7, 8, 9, 23, and 45, for example). The cycle then begins again with another terrigenous lamina.

There are minor variations in the types of diatoms that appear within the succession in each varve. The succession is most prevalent in the thicker varves (1–26) in the bottom half of the slab. In these successions, the different diatomaceous lamina components are clearly demarcated (Appendix A, slides A–C). The taxonomic succession is less pronounced in the thinner varves (27–56). Here, the discrete *Thalassiosira*, *Skeletonema* and *Chaetoceros* sublaminae are reduced in thickness or are lacking, and the silty diatomaceous laminae are thicker (Appendix A, slides D and E).

5.3. Nonlaminated intervals

There are three ~1-cm thick nonlaminated intervals situated at the bottom, middle and top of the slab (Fig. 2), referred to as NL-B, NL-M and NL-T, respectively. Each nonlaminated interval has sharp and bedding-parallel contacts, and a massive texture and brown color when viewed without magnification. In thin section, NL-B and NL-T display a mottled texture (Appendix A, Slides A and E), whereas NL-M also displays a mottled texture yet also contains indistinct laminae (Appendix A, Slide C). Up to four varves may be represented by the indistinct laminae, giving a possible total of up to 66 years of deposition throughout the slab. However, since it was difficult to sample these varves individually, bulk samples were taken. Each nonlaminated interval is composed of a mixture of silt, organic debris, diatom remains and millimeter-scale blebs of various compositions. The blebs display platy alignment oriented with the bedding plane (Appendix A). NL-M and NL-T also contain unidentified benthic foraminifera.

5.4. Interannual diatom abundance and assemblages

The mean abundance of diatoms counted from all 67 samples is estimated at 4.5×10^8 valves/g of dry sediment (Fig. 2E). The mean abundance of *Chaetoceros* resting spores (CRS) is estimated at 1.3×10^8 valves/g. There is a general decrease in diatoms toward the top of the slab, following the thinning upward pattern of the varves (Fig. 2E). Mean diatom abundance in the thicker varves (samples S8-42 to S8-67, excluding the sample from NL-B) is estimated at 5.5×10^8 valves/g. Diatom abundance is greatly reduced in varves 8 and 9 (samples S8-60 and S8-59, respectively). The sharp decrease in diatoms from varve 8 can be explained by a sublamina enriched in an unknown, unidentifiable microfossil that was not counted as a diatom (Appendix A, Slide B). The abundance of this unknown morphology diluted the diatom signal. In the thinner varves (samples S8-1 to S8-37, excluding samples from NL-T, NL-M and indistinct varves), the mean diatom abundance is estimated at 4.0×10^8 valves/g. CRS abundance shows a very slight upward decreasing trend, with a mean abundance of 1.5×10^8 valves/g in the thicker varves and 1.2×10^8 valves/g in the thinner varves.

The weakly silicified form of *S. costatum* is the most dominant taxon in the bottom portion of the slab, with a maximum relative abundance of 82% and absolute abundance of 9.5×10^8 valves/g (Figs. 4 and 5). Other dominant diatoms, all of which have an absolute abundance greater than 1×10^8 valves/g are, in order of decreasing abundance, *S. costatum* (nominal, robust form), *Thalassiosira nordenskioeldii*, *Thalassiosira decipiens*, and *Fragilariopsis pseudonana* (Fig. 5). Other dominant taxa include *T. nitzschioides* (maximum abundance 9.6×10^8 valves/g) and *Thalassiosira pacifica* (maximum abundance 8.5×10^8 valves/g) (Figs. 4 and 5).

Although the overall diatom abundance shows a general decrease as varves become thinner toward the top of the slab, a comparison between brackish water and benthic diatoms with marine planktic diatoms shows that many brackish water and benthic taxa increase in abundance in the thinner varves. Average estimates of total brackish water and benthic diatoms yield 4.1×10^7 valves/g for the thicker varves and 5.7×10^7 valves/g for the thinner varves. Taxa such as *Achnanthes minutissima*, *Cocconeis scutellum*, *Navicula perminuta*, *Nitzschia frustulum*, *Planothidium delicatulum*, and *Paralia sulcata* show definite increases in both relative and absolute abundance in thinner varves (Figs. 4 and 5).

Benthic and brackish water taxa also dominate the assemblage in NL-T (Figs. 4 and 5). Taxa such as *P.*

delicatulum, *P. sulcata* and *N. frustulum* are slightly elevated in abundance in this interval. The planktic brackish water species *Cyclotella choctawhatcheeana* shows an increase in NL-M. There are also slight increases in marine taxa *S. costatum* (nominal form), *Fragilariopsis pseudonana* and *Thalassiosira decipiens* in this interval. Marine diatom taxa dominate the assemblage in NL-B (Fig. 4).

6. Discussion

6.1. Seasonal components of varves

The individual lamina types in Slab 8 represent discrete seasonal deposition. A succession of discrete near-monospecific sublaminae containing *Thalassiosira* species, *S. costatum,* and/or CRS represents the individual stages of the spring bloom. From modern trap studies, *Thalassiosira* spp. often begin the bloom because they respond to increased sunlight early in spring while the surface waters are still cool (Waite et al., 1992; Chang, 2004). *S. costatum* and CRS follow as water temperatures rise. In some varves, even though these taxa may not occur in discrete sublaminae, these three taxa are often the first to appear above the terrigenous winter lamina. This spring assemblage agrees with Stage I of the seasonal succession for coastal planktic diatoms defined by Margalef (1958).

Mixed-species laminae overlie the near-monospecific sublaminae. The mixed species laminae contain a high diversity of taxa that are usually found during the summer months, as was observed in sediment trap studies within Effingham Inlet (Chang, 2004). The assemblage represented in mixed-species laminae agrees with Stage II of Margalef's succession. The assemblage in silty diatomaceous laminae, which overlie mixed-species laminae and underlie terrigenous laminae, contains a high diversity of diatoms as well, but with the presence of increased silt and debris, as well as the appearance of silicoflagellates. Dinoflagellate cysts were found only in varve 10, but have been described in this lamina type from thin section analysis of other slabs taken from the same core (Chang et al., 2003). The increased silt and debris can be attributed to increased precipitation in the autumn, which delivers material from the sides and marshes of the fjord to the basin. Silicoflagellates have been described from late summer and autumn sediment trap samples from Saanich Inlet (Sancetta, 1989) and Santa Barbara Basin (Lange et al., 1997), and dinoflagellates were observed in the autumn in Jervis Inlet (Sancetta, 1989). The description of silty diatomaceous laminae is consistent with Stage III of Margalef's seasonal succession.

The near-monospecific laminae found intercalated within silty diatomaceous laminae may represent deposition from a late summer or early autumn production event. Sancetta (1989) found a distinct autumn (September to October) assemblage in Saanich Inlet, consisting of *T. nitzschioides*, *Rhizosolenia* spp., *S. costatum*, and several species of *Chaetoceros*. Larger diatoms occurring at this time of year are likely able to grow slowly under nutrient-poor, low-light conditions, or can regulate their buoyancy to acquire nutrients at depth (Guillard and Kilham, 1977; Kemp et al., 2000). These late summer and early autumn laminae may represent deposition of what Kemp et al. (2000) call "fall dump" assemblages. Alternatively, periodic disturbances to the stratified waters (i.e., by storms or strong winds) can return nutrients to the surface and lead to diatom miniblooms (Harrison et al., 1983; Haigh et al., 1992).

The succession described above mainly applies to the strong seasonality represented in the thicker varves of Slab 8. The similarity between the Effingham Inlet diatom succession and successions observed from other northern hemisphere temperate coastal areas suggests that many of these dominant diatom species are responding to similar physical cues for production at around the same time of year (Dean et al., 2001).

6.2. Interannual varve variability

Analysis of Slab 8 from Figs. 2 and 3 shows that the average thickness of terrigenous laminae is reduced by 21% as varve thickness decreases toward the top of the slab, but that the diatomaceous laminae have a reduction of 37%, causing overall varve thickness to decrease. A study of sediment trap samples from Effingham Inlet shows that terrigenous input is greatest during the autumn and winter (Chang, 2004). Thus, the minor interannual variability in the thickness of the terrigenous laminae throughout the slab suggests that autumn and winter terrigenous input into

the inner basin was relatively the same, or decreased slightly, throughout the 62 or so years of deposition. However, silt content within the diatomaceous laminae, as determined from thin section analysis, gradually increased over time. This suggests that seasonality became weaker as the spring and summer seasons became wetter, delivering more terrigenous debris to the basin at these times of the year. The amount of rainfall is positively correlated to the amount of detritus washed into the fjord from runoff, as was evident in the sediment trap studies in Effingham Inlet (Chang, 2004) and in other sites where hemipelagic sediments accumulate (e.g., Santa Barbara Basin, Soutar and Crill, 1977). Hence, it is suggested that a progressive increase in precipitation over time led to increased continental runoff and delivery of terrigenous debris into the basin, resulting in a higher silt and terrigenous debris content in the thinner varves.

The absolute abundance of total diatoms and CRS can be used as a proxy of production. The abundance shows a progressive decrease toward the top of the slab in concert with decreasing varve thickness. This decrease in diatom abundance is governed by the amount of the dominant taxon *S. costatum* (weak form). *S. costatum* is a species often described from coastal and fjord settings throughout the northern hemisphere (e.g., Lange et al., 1992) and responds to seasonal upwelling. The decrease in *S. costatum* over the 62 years suggests a reduction in nutrient delivery that likely resulted from weakened upwelling over time.

Imprinted on this overall decrease in total diatom abundance is the slight increase in the abundance of various brackish water and benthic species. Along with the increase in silt content in the thinner varves, the increase in benthic and brackish water species over time may also signal a response to increased precipitation and runoff. Taxa such as *Achnanthes minutissima*, *Navicula perminuta*, *Paralia sulcata* and *Planothidium delicatulum* are more common in thinner varves (Fig. 5). These taxa can be easily sloughed off from benthic habitats along the margins of the fjord or in marsh areas during storm activity or heightened runoff caused by increased rainfall (McQuoid and Hobson, 1998). Likewise, these taxa may have opportunistically flourished in the fjord when surface salinities along the margins were lowered due to the increased precipitation. Another possible explanation for the observed increase in benthic species is a rise in sea level (McQuoid and Hobson, 1998). This can cause flooding of shallow areas along the margins of the fjord, increasing the available habitat for benthic species. Although sea level has deviated no more than a few meters during the last 5000 years, and these regional fluctuations are relatively minor when compared to those following the deglacial period (Clague, 1989), it is difficult to determine from the sediment slab alone whether there was a sea level increase throughout the time when benthic taxa increased in numbers. A more detailed local study of sea level fluctuations would be required to resolve this.

6.3. Interpretation of nonlaminated intervals

Although the three nonlaminated intervals in the slab have a similar physical appearance macroscopically, the origins of each interval are likely to be different, due to their differing diatom assemblages. NL-B contains abundant *S. costatum* and other marine diatoms. The relative abundance of these diatoms is similar to the diatom proportions from varves immediately above and below this nonlaminated interval (Fig. 4). This interval could represent normal laminated sediment deposition interrupted by an oxygenation event caused by a seawater incursion whereby increased oxygen levels introduced bioturbating macrobenthos to the bottom waters (Schimmelmann et al., 1992; Dallimore, 2001). Bioturbation of the sediments would then disrupt the original sedimentary laminae and homogenize the sediment. However, other than homogenized sediment, there are no obvious indications of bioturbation, in the form of burrows or remains of the bioturbating organisms themselves, either within NL-B or in the varves below, as has been observed in other bioturbated laminated sediments (e.g., Grimm and Föllmi, 1994; Chang and Grimm, 1999). Alternatively, the intrusion of bottom-hugging oxygenated water entering the fjord may have had enough momentum to disturb, mix and resettle sediment, resulting in the massive texture of NL-B (A. Dallimore, pers. comm.). The platy alignment of blebs within NL-B supports the mechanism of grain settling from suspension since bioturba-

tion would have resulted in the in situ churning of sediments and randomization of grain orientation (Govean and Garrison, 1981).

Intervals NL-M and NL-T contain an increased abundance of benthic, brackish diatom taxa, such as *Achnanthes minutissima*, *Navicula perminuta*, *Nitzschia frustulum*, *Paralia sulcata* and *Planothidium delicatulum*. The increase in these taxa likely reflects similar conditions that were responsible for the increase in these taxa in the upper portion of the slab in general. The increase of the planktonic brackish water species *Cyclotella chochtawhatcheeana* in NL-M can also be explained by an increase in freshwater input, which would have lowered surface salinities over the inner basin, enough for this taxon to temporarily dominate in the area. The appearance of this taxon apparently reflects higher amounts of precipitation (M. Hay, pers. comm.). The amount of material represented in NL-M and NL-T, and the elevated amount of benthic and brackish water species, may have resulted from extraordinary precipitation events and resultant flooding and delivery of debris over and into the inner basin. The appearance of four indistinct varves within NL-M suggests that there may have been up to four years of increased rainfall and terrigenous input and especially low seasonality at this time.

6.4. Climatic interpretations

What could cause the decrease in coastal marine species and seasonality of the varves, and the increase in silt and benthic taxa over the span of 62 years? The answer may be linked to changes in the intensities of atmospheric pressure systems over time.

Upwelling and production along the British Columbia coast are highly seasonal and governed by the positions of the AL and NPH pressure systems. The AL dominates the north Pacific during the autumn and winter resulting in southeasterly winds, shoreward movement of surface waters, downwelling and reduced primary production. The AL also brings more cloudy weather and precipitation, conditions that are standard for coastal British Columbia during this time of the year. In the spring and summer, however, the NPH pressure system moves northward and dissipates the AL, leading to northwesterly winds, upwelling, increased primary production, sunnier skies and less precipitation.

The evidence provided in Slab 8 suggests that above varve 26, where varves become more silty and the abundance of marine coastal diatom taxa decreases, the AL gradually strengthened or persisted for a longer interval during the year. Alternatively, the NPH may have become weaker or did not move as far north during the summer to initiate upwelling along the British Columbia coast. A combination of both of these factors may also compound the situation. An examination of the sediments immediately below Slab 8 indicates that the sediments in Slab 8 record a transitional period from a time of high seasonality to a time of low seasonality. Varves from at least 17 cm of sediment (~60 years) below Slab 8 are thick (2–3 mm) and display distinct seasonal lamina components (Chang et al., 2003, Chang, 2004). Therefore it appears that there were at least some 80 years of drier, high seasonality conditions before the wetter, low seasonality conditions set in, and that the climate shift occurred within a couple of decades.

Recent research suggests that the changing intensities and locations of the AL and NPH may reflect a higher-order forcing factor. Christoforou and Hameed (1997) and Hameed and Lee (2003) have observed that the positions of the AL and NPH are related to solar activity, namely the 11-year Schwabe sunspot cycle. They determined that during sunspot maxima, the AL system moves west by as much as 700 km while the NPH moves north by as much as 300 km. These systems move in the opposite way during sunspot minima. Other longer cycles, such as the 20–22-year Hale cycle and the 72–90-year Gleissberg cycle (Dean, 2000), both of which are modulations of the 11-year cycle, may produce a similar effect on the locations of the AL and NPH (Patterson et al., 2004a,b). There is now a growing body of evidence that suggests that celestial and solar factors are at least partially responsible for climate variability from daily to millennial time scales (e.g., Friis-Christensen and Lassen, 1991; Haigh, 1994; Soon et al., 1996; Svensmark, 1998; Bond et al., 2001; Carslaw et al., 2002). A detailed discussion of the mechanistic pathways are described elsewhere (e.g., Svensmark and Friis-Christensen, 1997; Marsh and Svensmark, 2000; Carslaw et al., 2002), but a simplified relationship would indicate that celestial and solar cycles drive climate and the positions of the AL and NPH, which in turn

determine patterns of precipitation and upwelling along the coast, which ultimately result in productivity and sedimentary cycles (Patterson et al., 2004a,b).

Perhaps the trends in Slab 8 reflect climate shifts not unlike those documented in the north Pacific from 1870 to 1997 (Mantua et al., 1997; Minobe, 1997, 1999) that are related to the Pacific Decadal Oscillation (Ebbesmeyer et al., 1989; Biondi et al., 2001). During these regime shifts, such as the well-documented 1976/1977 shift, the climate over the north Pacific switches from being warm and AL-dominated to cool and NPH-dominated. Biological activity (e.g., primary production and fish migration patterns) follows accordingly (Chavez et al., 2003), resulting in economic disaster when fish populations do not reappear when anticipated (Mantua et al., 1997). It appears that the placement of the AL, displaced either eastward or westward, is important in determining whether the British Columbia coast becomes warmer or cooler, or receives more or less precipitation (Cayan and Peterson, 1989; Gershunov et al., 1999; review in Dean and Kemp, 2004). The trends in Slab 8 indicate that AL-related climate shifts have been operating since at least the late Holocene and are recurring phenomena. Minobe (1999) noted that the modern regime shifts went from one extreme to the other over a period of 25–35 years, giving a 50–70 year climatic oscillation. It appears that the 80-year climate regime represented by Slab 8 and the sediments below are two to three times longer than the regimes witnessed from the late 19th to 20th centuries. Spectral analysis of data from Slab 8 should be able to reveal these and other climate cycles such as El Niño/La Niña and the quasi-biennial oscillation (cf. Dean and Kemp, 2004).

7. Conclusion

Sediment texture, composition and diatom assemblages were determined at subseasonal to interannual scales. The stratigraphy of Slab 8 from Effingham Inlet suggests that major environmental change can occur within a couple of decades after a relatively prolonged period of climatic stability. The progressive decrease in the thickness of the varves and changes in diatom assemblages indicate that the production of marine species, and the environmental factors that support them, deteriorated over time. The concomitant increases in silt and benthic taxa point toward enhanced precipitation and continental runoff into the basin. The causal factor behind this kind of climate and environmental shift likely involves large-scale changes in the ocean–atmosphere system, namely a transition from a climate phase dominated by the NPH to one dominated by the AL. The bidecadal-scale climate shift at ~4400 years BP, along with shifts observed throughout the 20th century, indicates that these shifts, whether long or short, rapid or gradual, appear to be commonplace events.

Acknowledgments

We are grateful for the assistance of researchers and staff from the Institute of Ocean Sciences and the Geological Survey of Canada (Ottawa and Pacific offices), and the staff and crew of the CCGS *John P. Tully.* Two anonymous reviewers helped to improve this manuscript. Support for this project was provided by a Natural Sciences and Engineering Research Council (NSERC) strategic project grant and a grant from the Canadian Foundation for Climatic and Atmospheric Sciences (CFCAS) to R.T.P. Grants from the Cushman Foundation for Foraminiferal Research and the Geological Society of America Student Research Program were provided to A.S.C.

Appendix A

Photomicrographs of thin section slides. Each image is best viewed from bottom to top, following depositional succession and varve labels (numbered intervals). Generally, terrigenous laminae are dark colored, and diatomaceous laminae are light coloured. Specific lamina types are represented by the corresponding rectangular bar: black = terrigenous lamina, white = near-monospecific lamina, gray = mixed-species lamina, gray stippled = silty diatomaceous lamina or nonlaminated interval. Major com-

ponents for each lamina type are listed, with the most abundant component (≥50% per field of view per lamina type) listed first (Chang et al., 2003). Millimeter-diameter dark circles or circular outlines on the thin section image are bubbles in the epoxy.

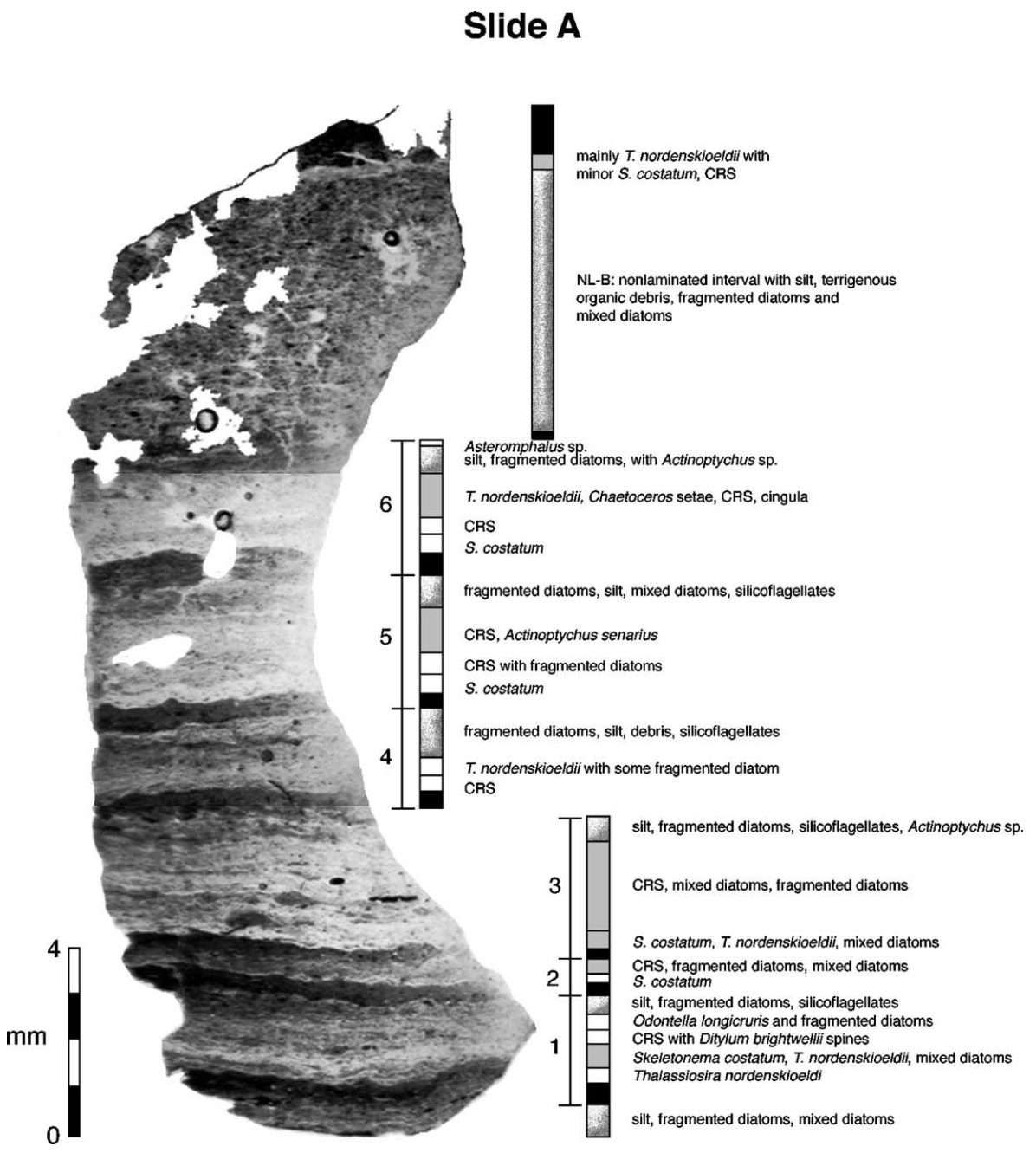

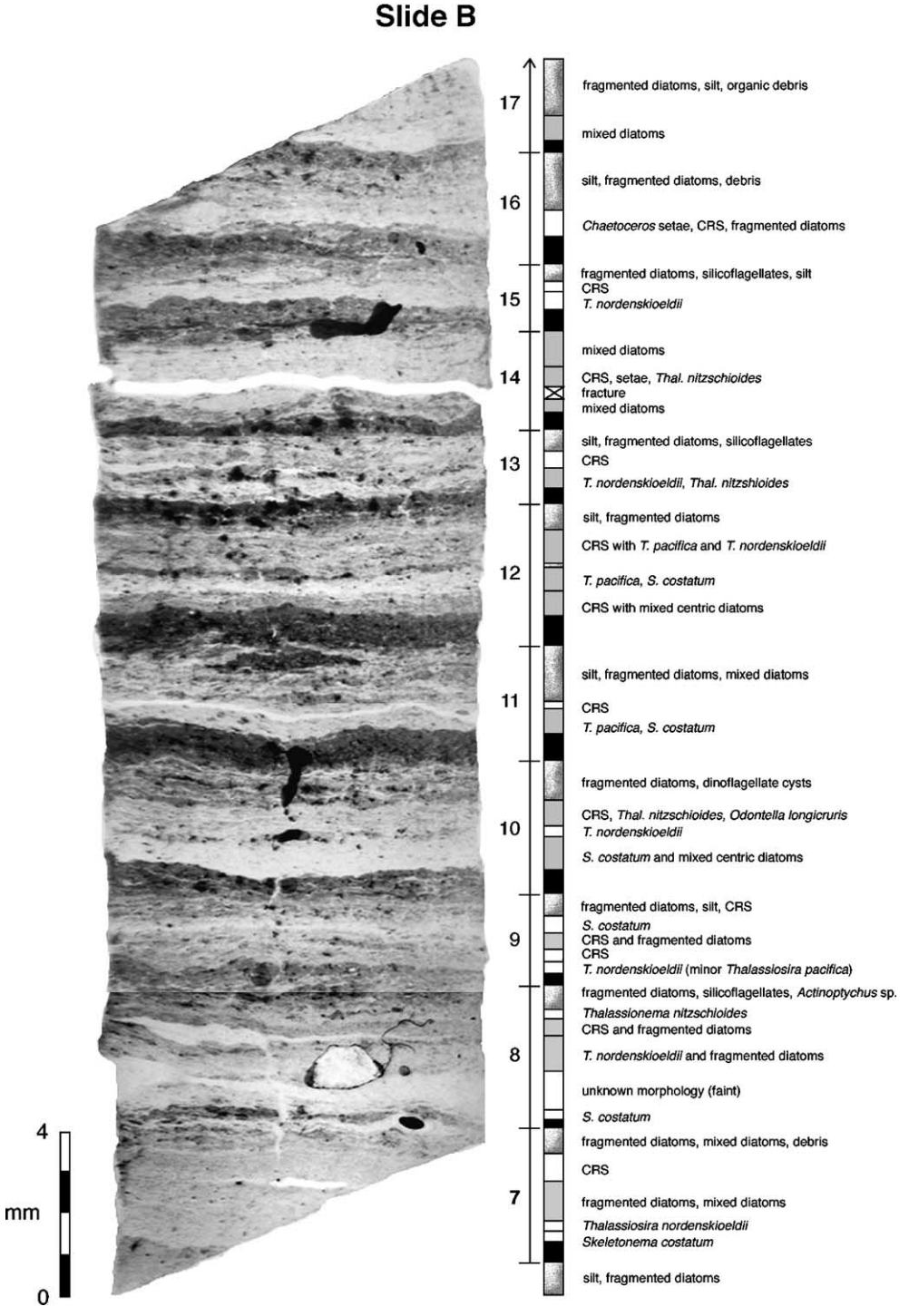
Slide B
17
fragmented diatoms, silt, organic debris
mixed diatoms
16
silt, fragmented diatoms, debris
Chaetoceros setae, CRS, fragmented diatoms
15
fragmented diatoms, silicoflagellates, silt
CRS
T. nordenskioeldii
14
mixed diatoms
CRS, setae, Thal. nitzschioides
fracture
mixed diatoms
13
silt, fragmented diatoms, silicoflagellates
CRS
T. nordenskioeldii, Thal. nitzshioides
12
silt, fragmented diatoms
CRS with T. pacifica and T. nordenskioeldii
T. pacifica, S. costatum
CRS with mixed centric diatoms
11
silt, fragmented diatoms, mixed diatoms
CRS
T. pacifica, S. costatum
10
fragmented diatoms, dinoflagellate cysts
CRS, Thal. nitzschioides, Odontella longicruris
T. nordenskioeldii
S. costatum and mixed centric diatoms
9
fragmented diatoms, silt, CRS
S. costatum
CRS and fragmented diatoms
CRS
T. nordenskioeldii (minor Thalassiosira pacifica)
8
fragmented diatoms, silicoflagellates, Actinoptychus sp.
Thalassionema nitzschioides
CRS and fragmented diatoms
T. nordenskioeldii and fragmented diatoms
unknown morphology (faint)
S. costatum
7
fragmented diatoms, mixed diatoms, debris
CRS
fragmented diatoms, mixed diatoms
Thalassiosira nordenskioeldii
Skeletonema costatum
silt, fragmented diatoms
4
mm
0

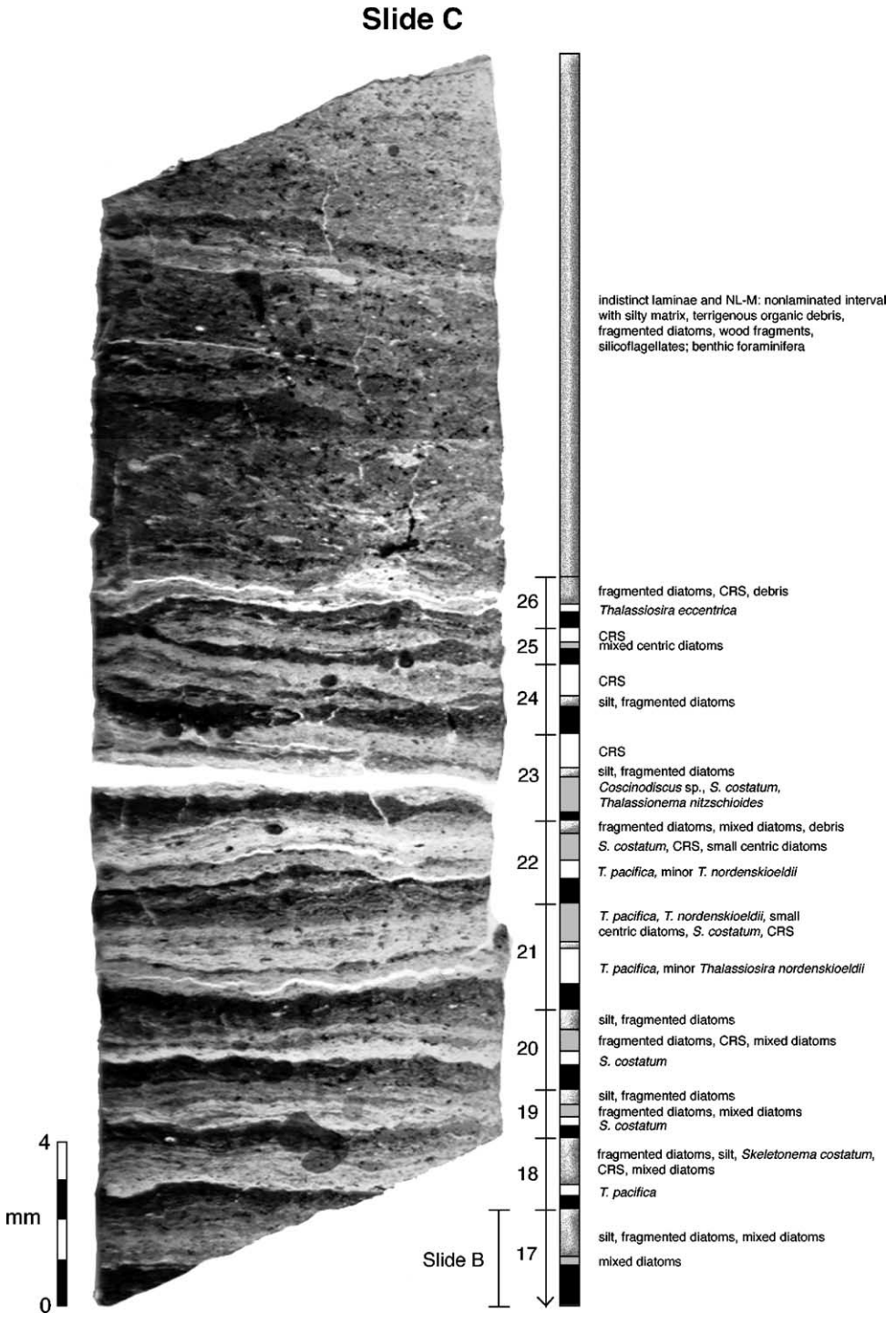
Slide C
indistinct laminae and NL-M: nonlaminated interval with silty matrix, terrigenous organic debris, fragmented diatoms, wood fragments, silicoflagellates; benthic foraminifera
26
fragmented diatoms, CRS, debris
Thalassiosira eccentrica
25
CRS
mixed centric diatoms
24
CRS
silt, fragmented diatoms
23
CRS
silt, fragmented diatoms
Coscinodiscus sp., S. costatum, Thalassionema nitzschioides
22
fragmented diatoms, mixed diatoms, debris
S. costatum, CRS, small centric diatoms
T. pacifica, minor T. nordenskioeldii
21
T. pacifica, T. nordenskioeldii, small centric diatoms, S. costatum, CRS
T. pacifica, minor Thalassiosira nordenskioeldii
20
silt, fragmented diatoms
fragmented diatoms, CRS, mixed diatoms
S. costatum
19
silt, fragmented diatoms
fragmented diatoms, mixed diatoms
S. costatum
18
fragmented diatoms, silt, Skeletonema costatum, CRS, mixed diatoms
T. pacifica
17
silt, fragmented diatoms, mixed diatoms
mixed diatoms
Slide B
4
mm
0

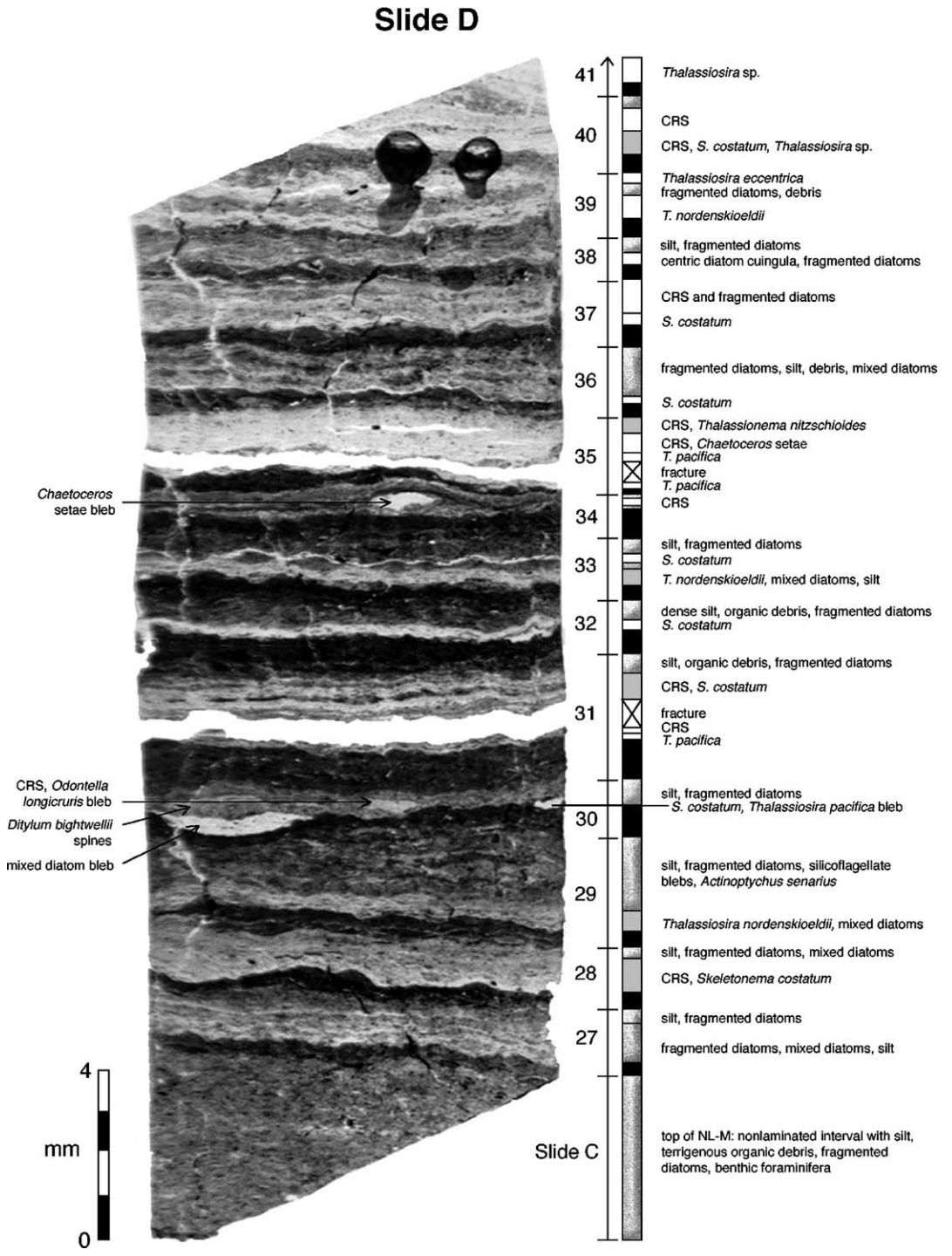
Slide D
41
40
39
38
37
36
35
34
33
32
31
30
29
28
27
Thalassiosira sp.
CRS
CRS, S. costatum, Thalassiosira sp.
Thalassiosira eccentrica
fragmented diatoms, debris
T. nordenskioeldii
silt, fragmented diatoms
centric diatom cuingula, fragmented diatoms
CRS and fragmented diatoms
S. costatum
fragmented diatoms, silt, debris, mixed diatoms
S. costatum
CRS, Thalassionema nitzschioides
CRS, Chaetoceros setae
T. pacifica
fracture
T. pacifica
CRS
silt, fragmented diatoms
S. costatum
T. nordenskioeldii, mixed diatoms, silt
dense silt, organic debris, fragmented diatoms
S. costatum
silt, organic debris, fragmented diatoms
CRS, S. costatum
fracture
CRS
T. pacifica
silt, fragmented diatoms
S. costatum, Thalassiosira pacifica bleb
silt, fragmented diatoms, silicoflagellate blebs, Actinoptychus senarius
Thalassiosira nordenskioeldii, mixed diatoms
silt, fragmented diatoms, mixed diatoms
CRS, Skeletonema costatum
silt, fragmented diatoms
fragmented diatoms, mixed diatoms, silt
Chaetoceros setae bleb
CRS, Odontella longicruris bleb
Ditylum bightwellii spines
mixed diatom bleb
4
mm
0
Slide C
top of NL-M: nonlaminated interval with silt, terrigenous organic debris, fragmented diatoms, benthic foraminifera

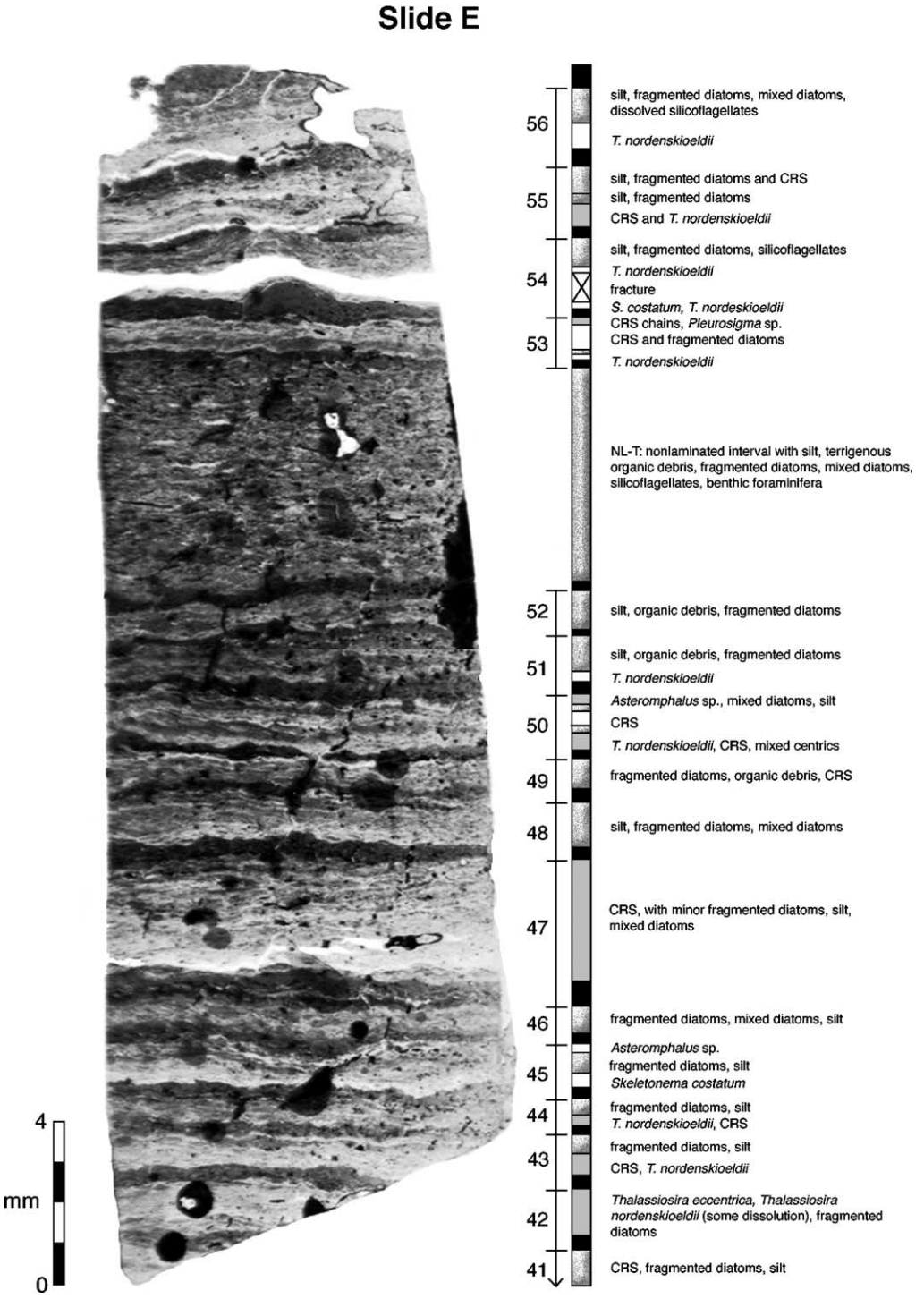
Slide E
4
mm
0
56
silt, fragmented diatoms, mixed diatoms, dissolved silicoflagellates
T. nordenskioeldii
55
silt, fragmented diatoms and CRS
silt, fragmented diatoms
CRS and T. nordenskioeldii
54
silt, fragmented diatoms, silicoflagellates
T. nordenskioeldii
fracture
S. costatum, T. nordeskioeldii
53
CRS chains, Pleurosigma sp.
CRS and fragmented diatoms
T. nordenskioeldii
NL-T: nonlaminated interval with silt, terrigenous organic debris, fragmented diatoms, mixed diatoms, silicoflagellates, benthic foraminifera
52
silt, organic debris, fragmented diatoms
51
silt, organic debris, fragmented diatoms
T. nordenskioeldii
50
Asteromphalus sp., mixed diatoms, silt
CRS
T. nordenskioeldii, CRS, mixed centrics
49
fragmented diatoms, organic debris, CRS
48
silt, fragmented diatoms, mixed diatoms
47
CRS, with minor fragmented diatoms, silt, mixed diatoms
46
fragmented diatoms, mixed diatoms, silt
45
Asteromphalus sp.
fragmented diatoms, silt
Skeletonema costatum
44
fragmented diatoms, silt
T. nordenskioeldii, CRS
43
fragmented diatoms, silt
CRS, T. nordenskioeldii
42
Thalassiosira eccentrica, Thalassiosira nordenskioeldii (some dissolution), fragmented diatoms
41
CRS, fragmented diatoms, silt

References

Bérard-Therriault, L., Poulin, M., Bossé, L., 1999. Guide d'identification du phytoplankton marin de l'estuaire et du Golfe du Saint-Laurent incluant également certains protozoaires. Publication spéciale canadienne de sciences halieutiques et aquatiques, vol. 128. Conseil national de recherches du Canada, Ottawa. 387 pp.

Biondi, F., Gershunov, A., Cayan, D.R., 2001. North Pacific decadal climate variability since 1661. Journal of Climate 14, 5–10.

Bond, G., Kromer, B., Beer, J., Muscheler, R., Evans, M.N., Showers, W., Hoffmann, S., Lotti-Bond, R., Hajdas, I., Bonani, G., 2001. Persistent solar influence on North Atlantic climate during the Holocene. Science 294, 2130–2136.

Campeau, S., Pienitz, R., Héquette, A., 1999. Diatoms from the Beaufort Sea Coast, Southern Arctic Ocean (Canada): Modern Analogues for Reconstructing Late Quaternary Environments and Relative Sea Levels. Bibliotheca Diatomologica, vol. Band 42. J. Cramer in der Gebrüder Borntraeger Verlagsbuchhandlung, Berlin. 244 pp.

Carslaw, K.S., Harrison, R.G., Kirkby, J., 2002. Cosmic rays, clouds and climate. Science 298, 1732–1737.

Cayan, D.R., Peterson, D.H., 1989. The influence of North Pacific atmospheric circulation of steamflow in the west. Geophysical Monograph 55, 375–396.

Chang, A.S., 2004. Ultra-high resolution sediment analysis and diatom paleoecology from Effingham Inlet, British Columbia, Canada: implications for Late Holocene environmental change. PhD Thesis, Carleton University, Ottawa, Canada.

Chang, A.S., Grimm, K.A., 1999. Speckled beds: distinctive gravity-flow deposits in finely laminated diatomaceous sediments, Miocene Monterey Formation, California. Journal of Sedimentary Research 69, 122–134.

Chang, A.S., Patterson, R.T., McNeely, R., 2003. Seasonal sediment and diatom record from Late Holocene laminated sediments Effingham Inlet, British Columbia, Canada. Palaios 18, 477–494.

Chavez, F.P., Ryan, J., Lluch-Cota, S.E., Ñiquen, C.M., 2003. From anchovies to sardines and back: multidecadal change in the Pacific Ocean. Science 299, 217–221.

Christoforou, P., Hameed, S., 1997. Solar cycle and the and the Pacific 'centers of action'. Geophysical Research Letters 24, 293–296.

Clague, J.J., 1989. Quaternary sea levels (Canadian Cordillera). In: Fulton, R.J. (Ed.), Quaternary Geology of Canada and Greenland, Geology of Canada, vol. 1. Geological Survey of Canada, Ottawa, pp. 43–47.

Cumming, B.E., Wilson, S.E., Hall, R.I., Smol, J.P., 1995. Diatoms from British Columbia (Canada) Lakes and their Relationship to Salinity, Nutrients and other Limnological Variables. Bibliotheca Diatomologica, vol. Band 31. J. Cramer in der Gebrüder Borntraeger Verlagsbuchhandlung, Berlin. 207 pp.

Dallimore A., 2001. Late Holocene geologic, oceanographic and climate history of an anoxic fjord; Effingham Inlet, west coast Vancouver Island. PhD thesis, Carleton University, Ottawa, Canada.

Dean, W.E., 2000. The Sun and Climate. USGS Fact Sheet FS-0095-00.

Dean, J.M., Kemp, A.E.S., 2004. A 2100 year BP record of the Pacific decadal oscillation, El Niño Southern Oscillation and quasi-biennial oscillation in marine production and fluvial input from Saanich Inlet British Columbia. Palaeogeography, Palaeoclimatology, Palaeoecology 213, 207–229.

Dean, J.M., Kemp, A.E.S., Pearce, R.B., 2001. Palaeo-flux records from electron microscope studies of Holocene laminated sediments Saanich Inlet, British Columbia. Marine Geology 174, 139–158.

Ebbesmeyer, C.C, Coomes, C.A., Cannon, G.A., Bretschneider, D.E., 1989. Linkage of ocean and fjord dynamics at decadal period. AGU Geophysical Monograph 55, 399–417.

Favorite, F., Dodimead, A.J., Nasu, K., 1976. Oceanography of the subarctic Pacific region, 1960–71. International North Pacific Fisheries Commission Bulletin 33 (187 pp.).

Friis-Christensen, E., Lassen, K., 1991. Length of the solar cycle: an indicator of solar activity closely associated with climate. Science 254, 698–700.

Gershunov, A., Barnett, T.P., Cayan, D.R., 1999. North Pacific interdecadal oscillation seen as factor in ENSO-related North American climate anomalies. EOS, Transactions – American Geophysical Union 80 (3), 25.

Govean, F.M., Garrison, R.E., 1981. Significance of laminated and massive diatomites in the upper part of the Monterey Formation, California. In: Garrison, R.E., Douglas, R.G., Pisciotto, K.E., Isaacs, C.M., Ingle, J.C. (Eds.), The Monterey Formation and Related Siliceous Rocks of California. Society of Economic Paleontologists and Mineralogists, Los Angeles, pp. 181–198.

Grimm, K.A., Föllmi, K.B., 1994. Doomed pioneers: allochthonous crustacean tracemakers in anaerobic basinal strata, Oligo–Miocene San Gregario Formation, Baja California Sur, Mexico. Palaios 9, 313–334.

Guillard, R.R.L., Kilham, P., 1977. The ecology of marine planktonic diatoms. In: Werner, D. (Ed.), The Biology of Diatoms, Botanical Monographs, vol. 13. Blackwell Scientific Publications, Oxford, pp. 372–469.

Haigh, J., 1994. The role of stratospheric ozone in modulating the solar radiative forcing of climate. Nature 370, 544–546.

Haigh, R., Taylor, F.J.R., Sutherland, T.F., 1992. Phytoplankton ecology of Sechelt Inlet, a fjord system on the British Columbia coast: I. General features of the nano-and microplankton. Marine Ecology. Progress Series 89, 117–134.

Hameed, S., Lee, J.N., 2003. Displacements of the Aleutian low and the Hawaiian high pressure systems during the solar cycle. Eos Transactions, American Geophysical Union 84 (Fall Meeting Supplemental) (Abstract SH11E-03).

Harrison, P.J., Fulton, J.D., Taylor, F.J.R., Parsons, T.R., 1983. Review of the biological oceanography of the Strait of Georgia: pelagic environment. Canadian Journal of Fisheries and Aquatic Sciences 40, 1064–1094.

Hemphill-Haley, E., Fourtanier, E., 1995. A diatom record spanning 114,000 years from Site 893, Santa Barbara Basin. Proceedings of the Ocean Drilling Program, Scientific Results, vol. 146 (Part 2). College Station, Texas, pp. 223–249.

Kemp, A.E.S., Pike, J., Pearce, R.B., Lange, C.B., 2000. The "Fall dump"—a new perspective on the role of a "shade flora" in the annual cycle of diatom production and export flux. Deep-Sea Research. Part 2. Topical Studies in Oceanography 47, 2129–2154.

Lamoureux, S.F., 1994. Embedding unfrozen lake sediments for thin section preparation. Journal of Paleolimnology 10, 141–146.

Lange, C.B., Hasle, G.R., Syvertsen, E.E., 1992. Seasonal cycle of diatoms in the Skagerrak, North Atlantic, with emphasis on the period 1980–1990. Sarsia 77, 173–187.

Lange, C.B., Weinheimer, A.L., Reid, F.M.H., Thunell, R.C., 1997. Sedimentation patterns of diatoms, radiolarians, and silicoflagellates in Santa Barbara Basin, California. CalCOFI Report 38, 161–170.

Laws, R.A., 1983. Preparing strewn slides for quantitative microscopical analysis: a test using calibrated microspheres. Micropaleontology 29, 60–65.

Mantua, N.J., Hare, S.R., Zhang, Y., Wallace, J.M., Francis, R.C., 1997. A Pacific interdecadal climate oscillation with impacts on salmon production. Bulletin of the American Meteorological Society 78, 1069–1079.

Margalef, R., 1958. Temporal succession and spatial heterogeneity in phytoplankton. In: Traverso, A.A. (Ed.), Perspectives in Marine Biology. University of California Press, Berkeley, pp. 249–323.

Marsh, N.D., Svensmark, H., 2000. Low cloud properties influenced by cosmic rays. Physical Review Letters 85, 5004–5007.

McQuoid, M.R., Hobson, L.A., 1998. Assessment of palaeoenvironmental conditions on southern Vancouver Island, British Columbia, Canada, using the marine tychoplankter *Paralia sulcata*. Diatom Research 13, 311–321.

Minobe, S., 1997. A 50–70 year climatic oscillation over the North Pacific and North America. Geophysical Research Letters 24, 683–686.

Minobe, S., 1999. Resonance in bidecadal and pentadecadal climate oscillations over the North Pacific: role in climatic regime shifts. Geophysical Research Letters 26, 855–858.

Patterson, R.T., Guilbault, J.-P., Thomson, R.E., 2000. Oxygen level control on foraminiferal distribution in Effingham Inlet, Vancouver Island, British Columbia, Canada. Journal of Foraminiferal Research 30, 321–335.

Patterson, R.T., Prokoph, A., Chang, A.S., 2004a. Late Holocene sedimentary response to solar and cosmic ray activity influenced by climate variability in the NE Pacific. Sedimentary Geology 172, 67–84.

Patterson, R.T., Prokoph, A., Wright, C., Chang, A.S., Thomson, R.E., Ware, D.M., 2004b. Holocene solar variability and pelagic fish productivity in the NE Pacific Ocean. Palaeontologia Electronica 7 (1) (17 pp.).

Pickard, G.L., 1963. Oceanographic characteristics of inlets of Vancouver Island, British Columbia. Journal of Fisheries Research Board of Canada 20, 1109–1144.

Ryder, J.M., 1989. Climate (Canadian Cordillera). In: Fulton, R.J. (Ed.), Quaternary Geology of Canada and Greenland, Geology of Canada, vol. 1. Geological Survey of Canada, Ottawa, pp. 26–31.

Sancetta, C., 1989. Spatial and temporal trends of diatom flux in British Columbian fjords. Journal of Plankton Research 11, 503–520.

Schimmelmann, A., Lange, C.B., Berger, W.H., Simon, A., Burke, S.K., Dunbar, R.B., 1992. Extreme climatic conditions recorded in Santa Barbara Basin laminated sediments: the 1835–1840 *Macoma* event. Marine Geology 106, 279–299.

Schrader, H.J., Gersonde, G., 1978. Diatoms and silicoflagellates. Utrecht Micropaleontological Bulletins 17, 129–176.

Soon, W.H., Posamentier, E.S., Baliunas, S.L., 1996. Inference of solar irradiance variability from terrestrial temperature changes, 1880–1993: an astrophysical application of the sun–climate connection. Astrophysical Journal 472, 891–902.

Soutar, A., Crill, P., 1977. Sedimentation and climatic patterns in the Santa Barbara Basin during the 19th and 20th centuries. Geological Society of America Bulletin 88, 1161–1172.

Stuiver, M., Reimer, P.J., 1993. Extended ^{14}C database and revised CALIB radiocarbon calibration program. Radiocarbon 35, 215–230.

Stuiver, M., Reimer, P.J., Bard, E., Beck, J.W., Burr, G.S., Hughen, K.A., Kromer, B., McCormac, F.G., Plight, J., Spurk, M., 1998a. INTCAL 98 radiocarbon age calibration 24,000–0 cal BP. Radiocarbon 40, 1041–1083.

Stuiver, M., Reimer, P.J., Braziunas, T.F., 1998b. High-precision radiocarbon age calibration for terrestrial and marine samples. Radiocarbon 40, 1127–1151.

Svensmark, H., 1998. Influence of cosmic rays on Earth's climate. Physical Review Letters 81, 5027–5030.

Svensmark, H., Friis-Christensen, E., 1997. Variation of cosmic ray flux and global cloud coverage—a missing link in solar–climate relationships. Journal of Atmospheric and Solar–Terrestrial Physics 59, 1225–1232.

Thomson, R.E., 1981. Oceanography of the British Columbia Coast. Canadian Special Publication of Fisheries and Aquatic Sciences, vol. 56. Department of Fisheries and Oceans, Ottawa. 291 pp.

Thomson, R.E., Gower, J.F.R., 1998. A basin-scale oceanic instability event in the Gulf of Alaska. Journal of Geophysical Research 103 (C2), 3033–3040.

Thomson, R.E., Hickey, B.M., LeBlond, P.H., 1989. The Vancouver island coastal current: fisheries barrier and conduit. In: Beamish, R.J., MacFarlane, G.A. (Eds.), Effects of Ocean Variability on Recruitment and an Evaluation of Parameters Used in Stock Assessment Models, Canadian Special Publication of Fisheries and Aquatic Sciences, vol. 108. Department of Fisheries and Oceans, Ottawa, pp. 265–296.

Waite, A., Bienfang, P.K., Harrison, P.J., 1992. Spring bloom sedimentation in a subarctic ecosystem. Marine Biology 114, 131–138.

Witkowski, A., Lange-Bertalot, H., Metzeltin, D., 2000. Diatom Flora of Marine Coasts I, Iconographia Diatomologica Annotated Diatom Monographs, vol. 7. A.R.G. Gantner Verlag K.G, Berlin. 925 pp.